Transportation Geotechnics 49 (2024) 101444

Contents lists available at ScienceDirect

Transportation Geotechnics

journal homepage: www.elsevier.com/locate/trgeo

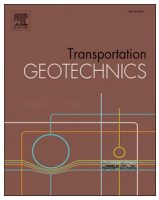

Evaluation of the elastic modulus improvement in geocell-reinforced unbound aggregates: Full-scale experimental sections on a highway

L.X. Feng [a,*], J.O. Avesani Neto [a], J.G. Zornberg [b]

[a] Department of Structural and Geotechnical Engineering, Escola Politécnica at the Universidade de São Paulo (EP-USP), São Paulo, SP, Brazil
[b] Department of Civil, Architectural and Environmental Engineering, The University of Texas at Austin, TX, USA

ARTICLE INFO

Keywords:
Geosynthetics
Modulus Improvement Factor (MIF)
Soil reinforcement
Pavement reinforcement
Deflection test

ABSTRACT

This article presents back analyzed results from experimental full-scale field test zones involving unreinforced and geocell-reinforced layers with unbound aggregate infill subjected to in-situ Benkelman Beam test (BBT). The field tests were conducted on experimental test zones during the construction of a new highway. Two types of Unbound Granular Materials (UGM), placed on layers of various thicknesses, were employed in unreinforced and geocell-reinforced pavement zones. Deflection measurements were collected for the different pavement structure layers using the BBT. The main objectives of the testing program were (1) to back calculate the elastic moduli on all test zones in both unreinforced and reinforced layers; (2) to determine the improvement in elastic modulus of the UGM, as quantified by the Modulus Improvement Factor (MIF), which results from geocell reinforcement; (3) to compare the measured MIF with MIF values reported in the literature under similar conditions; and (4) to evaluate the accuracy of available analytical methods to estimate the MIF. The results demonstrated a significant improvement in the elastic modulus of the UGM using geocell reinforcement, with MIF values ranging from 2.6 to 3.3, depending on the fill material. One analytical method used to calculate MIF values was found to have good predictive capability, confirming its potential to the design of pavements with geocell-reinforced layers.

Introduction

Geocells are geosynthetic products with civil engineering applications ranging from erosion protection to soil reinforcement [1–6,44]. Their implementation has increased in recent years due to their effectiveness in addressing various engineering problems, particularly those related to soil reinforcement for transportation infrastructure [7–11].

The improvement in the mechanical properties of aggregate infill can be attributed to the increased confinement provided by the geocells' honeycomb structure. Specifically, residual stresses are locked in within the cell pockets allowing the geocell-reinforced layer to behave as a prestressed concrete mat [12,13]. Besides providing lateral confinement, geocells can stiffen the Unbound Granular Material (UGM) pavement layer and thus improve its performance in pavement structures [14]. A parameter that accounts for the ability of a geocell to stiffen the aggregate layer is the Modulus Improvement Factor (MIF), defined as the ratio between the modulus in a geocell-reinforced soil to that in an unreinforced soil as shown in equation (1).

$$MIF = \frac{E_{ref}}{E_{un}} \tag{1}$$

The MIF could be determined using several experimental techniques, including small- and large-scale laboratory experiments; experimental full-scale tests track; back analysis of monitoring data from roads and railroads; and numerical simulations, such as Finite Element Analysis (FEA). Typically reported MIF values range from 1.5 to 5.0 in laboratory experiments, and from 2.0 to 3.5 in experimental full-scale tests and back analyses of field works [11,15–18]. Due to its usefulness in design, the use of the MIF is adequate for designing transportation infrastructure involving geocell reinforcement, as it allows for directly inputting the modulus of a reinforced layer in methods such as the Mechanistic-Empirical Pavement Design Method (MEPDM). An analytical method to estimate the MIF was recently developed by Garcia and Avesani Neto (2021) [13], which facilitates the simple incorporation of the geocell reinforcement in MEPDM analysis and in designs using the Layered Elastic Theory (LET) software.

Despite the MIF successful application to several transportation infrastructure projects, lack of information on the design and life cycle

* Corresponding author at: Escola Politécnica at the Universidade de São Paulo (EP-USP), 05508-010, Av. Professor Almeida Prado, travessa 2 no 83, São Paulo, SP, Brazil.
E-mail addresses: linfeng@usp.br (L.X. Feng), avesani@usp.br (J.O. Avesani Neto), zornberg@mail.utexas.edu (J.G. Zornberg).

https://doi.org/10.1016/j.trgeo.2024.101444
Received 21 May 2024; Received in revised form 11 September 2024; Accepted 13 November 2024
Available online 15 November 2024

Nomenclature

E	Elastic Modulus (Young's modulus) (MPa)
J	Geocell wall stiffness
Si	Stiffness Index.
υ	Poisson's ratio (dimensionless)
γ	Soil specific weight (kN/m^3)
ϕ'	Soil friction angle (°)
c'	Effective cohesion parameter (dimensionless)
k	Duncan et al. (1980) modulus number for loading (dimensionless)
ku	Duncan et al. (1980) modulus number for unloading (dimensionless)
n	Duncan et al. (1980) modulus exponent (dimensionless)
Rf	Duncan et al. (1980) failure ratio (dimensionless)

performance of geocell-reinforced flexible pavements has hindered its use. Currently, specific guidelines are not readily available for designing and constructing geocell-reinforced pavements, most likely due to the limited availability of field performance data. This limitation hinders the establishment of a comprehensive database for referencing the construction, post-construction, and long-term performance of such pavements under field conditions [19].

For addressing the need for field performance data on full-scale geocell systems, this study involves the back analysis of deflection results from Benkelman Beam Tests (BBT) on both unreinforced and geocell-reinforced UGM layers constructed within a highway pavement structure. Specifically, a full-scale field-testing program of highway test zones was undertaken to evaluate the improvements observed from geocell reinforcement to stiffen two typical UGM layers used as base and subbase in pavement structures. An LET-based software was employed to determine the modulus for both reinforced and unreinforced layers, enabling the quantification of geocell improvements in terms of MIF under field conditions. Comparisons were also made with the MIF analytical method used in highway design as well as with a similar MIF obtained by previous publications.

Experimental full-scale field test

A series of full-scale field test zones were installed in a highway under construction in the Brazilian southern region. The overall zone measured 170 m in length and 12 m in width and was divided into four test zones with an unreinforced and geocell-reinforced base and subbase layers. Each zone was designed to be 50 m in length to allow for a comprehensive evaluation of the deflectometer test using the Benkelman beam test (BBT).

Fig. 1 presents a plan view and a cross-section of the four zones evaluated in this study. Fig. 1A displays that zones 1, 2, and 3 were positioned in the same highway direction, with a distance of 10 m between each, while zone 4 was placed in the opposite highway direction. Fig. 1A and Fig. 1B show that zone 1 served as the control, comprising an unreinforced pavement structure consisting of a 250 mm subbase layer of crushed stone subbase (CSS) and a base layer with a height of 150 mm

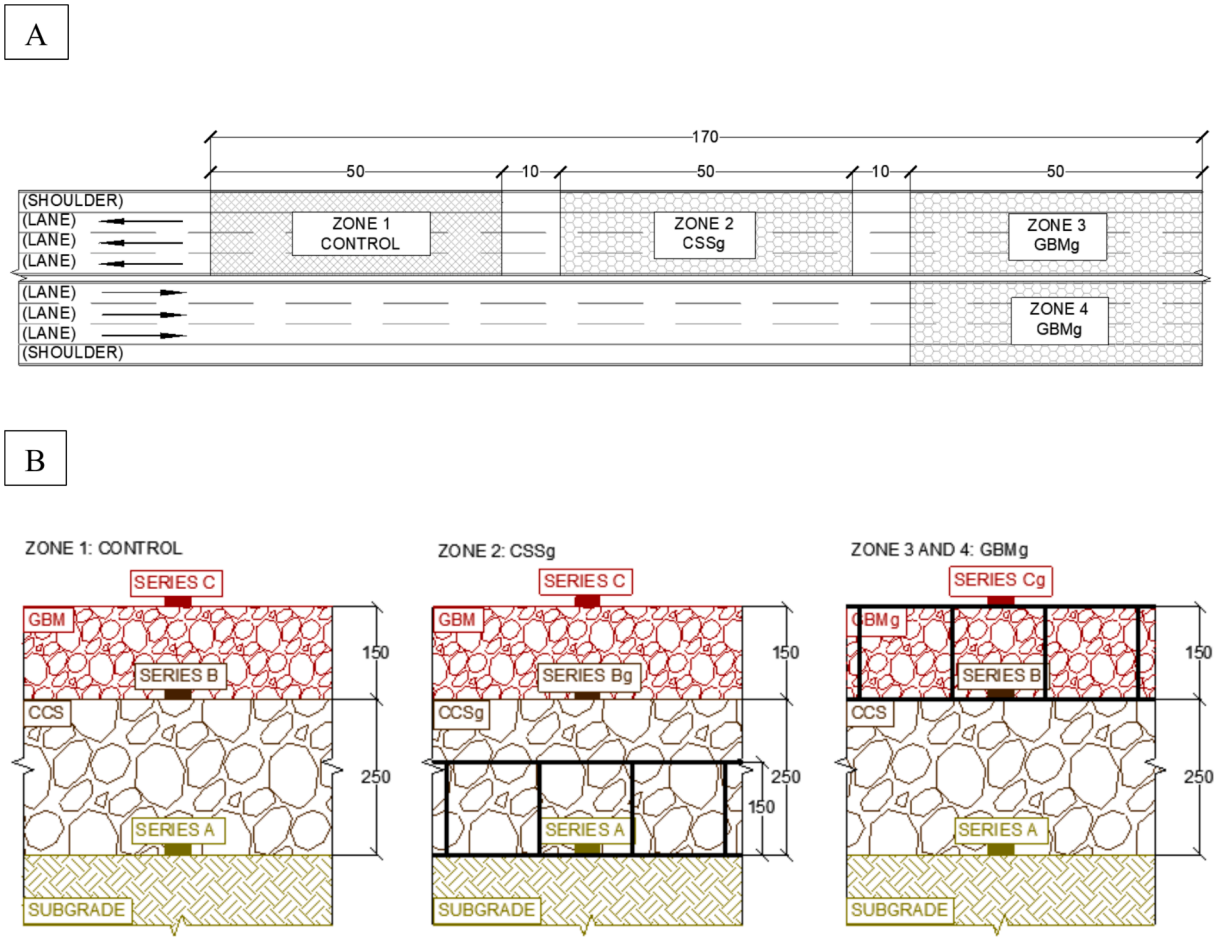

Fig. 1. Schematic illustration of the experimental full-scale field test zones. (A) Plan view with the position of the zones (dimensions in m). (B) Cross-sections indicating the layers thicknesses, the materials, the reinforcement, and the series of BBT conducted (dimensions in mm).

of granular base material (GBM). Zones 2, 3, and 4 were geocell-reinforced pavement structures (Fig. 1B). In zone 2, the geocell was placed in the subbase layer, resulting in a geocell-reinforced crushed stone subbase (CSSg – where 'g' denotes a geocell-reinforced layer). Zones 3 and 4 were constructed with the geocell positioned in the base layer, creating a geocell-reinforced granular base material (GBMg). Fig. 1B illustrates that all zones were designed using the same materials and thicknesses, differing only in the inclusion and positioning of the reinforcing layer. Additionally, Fig. 1B displays the positions of the BBT conducted in each structure layer, referred to as "series". Series A denotes the BBT performed directly over the local subgrade. Series B and C represent the BBT conducted respectively on the unreinforced subbase (CSS) and base (GBM) pavement layers. Series Bg and Cg indicate the BBT conducted respectively on the geocell-reinforced subbase (CSSg) and base (GBMg) pavement layers.

Subgrade

The test zones subgrade consisted of the in-situ material at the project site. The local subgrade is a lateritic silty clay, with its particle distribution curve presented in Fig. 2. The in-situ water content was determined to be 1.55 % at the time of construction, and the specific gravity of solids was measured at 2.77. Additionally, the Liquid Limit (LL) and Plasticity Index (PI) were determined to be 77 % and 40 %, respectively. The subgrade is classified as A-7–5 (9) according to the AASHTO Soil Classification System soil classification system, and high plasticity silty (MH) according to the Unified Soil Classification System (USCS).

Crushed stone subbase (CSS)

The subbase material corresponds to a well-graded aggregate, referred to as CSS. This material, commonly used for roadway subbase courses in Brazil, is often identified as macadam. Macadam is composed of angular fragments of crushed stones in various sizes, ranging in diameter from 12 to 85 mm, and is known for its good durability, resilience, and non-reactive characteristics. The CSS particle distribution curve is shown in Fig. 2. This material is classified as A-1-a according to the AASHTO Soil Classification System and GP according to the USCS.

Granular base material (GBM)

The base layer was a typical GBM composed of a graded base; its particle distribution curve is presented in Fig. 2. This material is classified as A-1-a and GW according to the AASHTO Soil Classification System and USCS Soil Classification Systems, respectively. The maximum dry density obtained was 2.18 kg/cm^3, with an optimum water content of 4.6 %, as determined by the compaction curve using samples from the local soil obtained in the laboratory Modified Proctor compaction test. Additionally, the California Bearing Ratio (CBR) test resulted in a value of 102 %.

Geocells

The specifications of the geocell reinforcement in both UGM layers were adopted as those reported by the manufacturer. The geocells were manufactured using High-Density Polyethylene (HDPE), measuring 150 mm in height, and had pocket sizes measuring 224 mm in width and 259 mm in length when fully opened, yielding an area of 0.0289 m^2. The cell walls were textured with holes punched in rows, each with a maximum diameter of 10 mm. The perforated area constitutes approximately 10 % of the total surface area of each cell. The HDPE elastic modulus under small strains was reported equal to 700 MPa. From the HDPE elastic modulus and the cell thickness, a tensile stiffness of 1155 kN/m was obtained.

Table 1 provides a summary of the geocell properties [22].

Construction of the full-scale test zones

All test zones were designed with identical layers, materials, and thicknesses, differing only in the placement of the geocell reinforcement.

Table 1
Summary of geocell properties.

Parameters	Value
Material	HDPE
Cell wall height (mm)	150
Expanded cell dimension (mm)	259 x 224
Cell open area (m^2)	0.0289
Equivalent diameter (mm)	192
Cell thickness (mm)	1.65
Geocell stiffness (kN/m)	1155

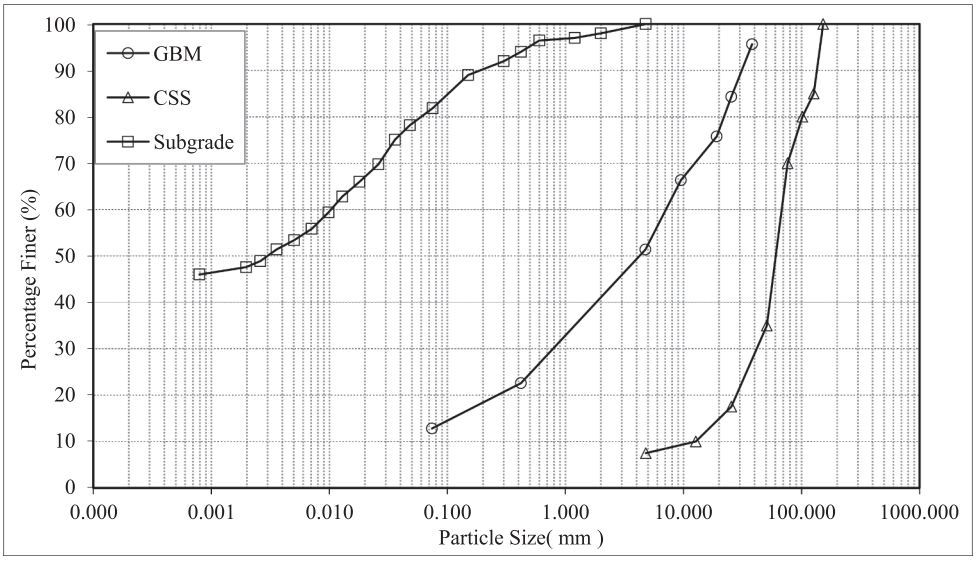

Fig. 2. Particle distribution curve of different materials.

This design approach facilitated the analysis and comparison of modulus improvements resulting from the geocell inclusion.

The zone 1 control involved an unreinforced UGM layer. The area was excavated until the project-defined subgrade level was reached and the initial BBT series was conducted, referred to as Series A in Fig. 1. Subsequently, a 250-mm-layer of CSS was placed and compacted, followed by the second BBT series (Series B). Finally, a 150-mm-layer of GBM was placed and compacted, and the third BBT series (Series C) was performed, concluding the testing of the zone 1 control.

The same procedures were followed for zone 2 and differed only in the incorporation of the geocell reinforcement in the CSS layer. The BBT tests performed on series A determined the deflections at the subgrade level; Series Bg was conducted on the 150-mm-thick geocell-reinforced CSS layer; and Series C was conducted on the 150-mm-thick GBM layer.

Zone 3 and zone 4 also followed similar procedures but with the geocell reinforcement positioned in the GBM layer. BBT tests performed on series A determined the deflections from BBTs at the subgrade level; Series B was conducted on the 250-mm-thick CSS layer; and Series Cg was conducted on the 150-mm-thick geocell-reinforced GBM layer.

Fig. 3 illustrates the installation steps of the geocell reinforcement in zone 3. Fig. 3A displays the aperture and positioning of the geocell panel. In Fig. 3B, the GBM is shown filling the geocell layer, while Fig. 3C depicts the compaction procedure. Fig. 2D presents conducting BBT over the geocell-reinforced granular base material (GBMg).

The test zones layers were compacted using a single smooth-drum vibratory roller measuring 2.1 m in width to compact both the CSS and GBM layers to 100 % of the maximum relative compaction, according to the Modified Proctor test. The compaction equipment made approximately four to eight passes to achieve the desired relative compaction and exerted a centrifugal roller drum force ranging between 133 and 234 kN. The compaction process and quality control (QC) strictly adhered to Brazilian standards, ensuring compliance with the required benchmarks for road construction. Quality management was conducted according to DNIT 011-PRO [20], which outlines the guidelines for quality management in road construction projects, ensuring that all stages of the project were properly monitored and controlled. Additionally, the statistical control methodology for construction and services was implemented following DNER-PRO 277 [21], which establishes procedures for verifying the uniformity and quality of compacted materials and assessing compliance with specified requirements.

The BBT is a simple and cost-effective deflection method, commonly employed in Brazil for construction quality control of all pavement structure layers in distinct transportation infrastructures. The BBT is also recommended for evaluating the benefits of geocell-reinforced pavement structure layers [26]. To conduct the tests, a Benkelman beam is positioned between the dual wheels of a Simple Axle Dual Wheel (SADT) vehicle and subjected to an 80 kN load and 560 kPa tire pressure, generating two equivalent circular loads spaced at a distance of 288 mm. All pavement layers have deflection criteria determined based on road characteristics and lifespan considerations, which BBT will measure. The BBT procedures adopted in this study adhered to both Brazilian and U.S. standards [27].

Results and discussion

Benkelman beam test deflection results

BBTs were conducted on the subgrade and on both unreinforced and

Fig. 3. Installation steps of geocell-reinforced zone 3: A) Geocell installation; B) Geocell filling; C) Layer compaction; and D) Deflection test (BBT).

reinforced layers, producing a total of 219 deflection measurements – approximately 55 in each zone and 25 in each series. Table 2 presents the BBT deflection ranges, averages, and Coefficient of Variation (COV) for each zone and layer.

The overview BBT results of all zones indicate deflections ranging from 0.59 to 6.29 mm, with a COV for each layer ranging between 9.5 and 36.3 %. As expected, higher deflections and maximum standard deviation were obtained on the subgrade surface, which is attributed to this less rigid layer and comparatively higher variability in soil characteristics. The BBT results indicate that the deflection of layers decreases as more layers are constructed, which is reflected in the decrease of both deflection and COV values. From the subgrade to the CSS layer, the deflections and COV decreased by approximately 50 % and 40 %, respectively. From the CSS to the GBM layer, the deflections decreased by approximately 25 % with no significant change observed in the COV. The lowest deflection and COV values were obtained for the geocell-reinforced layers, with a COV approximately 55 % lower than those obtained for the unreinforced layers. A COV evaluation reveals that the subgrade can be considered almost non-uniform, the unreinforced layers (CSS and GBM) can be classified as fair and the reinforced layers (CSSg and GMBg) can be considered very uniform [28]. The geocell reinforcement was able to adequately distribute the deflections across the layer and reduce its value.

The results in Table 2 indicate that the average deflection values between the unreinforced and reinforced layers did not show significant improvement when comparing Series B to Series Bg and Series C to Series Cg. As the deflection of upper layers is influenced by subgrade deformability, the results in Table 2 may not capture the improvement provided by the geocell, back analyses thus needs to be carried out using a layered elastic system. In the following section, the results of back analyzed elasticity moduli using multi-layered elastic system software will be presented.

Back analyses of layered elastic system

The deflections measured by the BBT are directly correlated with the displacements obtained from the Layered Elastic Theory (LET), which relates the stress and strain of the materials based on their elastic modulus, Poisson's coefficient, and layer thickness. Various approaches can be employed to back analize layer elastic moduli from these responses, including the use of software based on LET, Finite Element Analysis (FEA) or analytical solutions also based on LET [12,29,30].

In this study, ELLEA1 software was used to back analyze the BBT in each layer. ELLEA1 is an LET-based software capable of calculating displacements, stresses, and strains in up to five layers subjected to up to two circular surface loads [31]. This software has previously been used to analyze and evaluate road pavement structures, including those with a geosynthetic layer [32].

The methodology used herein followed that proposed by Avesani Neto and Rodrigues (2021) [23] and Zipoli and Avesani Neto (2022) [24]. The BBT results were obtained in an iterative process using the LET software. The input parameters included the thickness and Poisson's ratio for each layer, as well as the position, dimensions, and magnitude of the load applied during the BBT. The evaluations included back analyzing the surface modulus, or equivalent modulus, (E_{suf}) and the elastic modulus of each layer (E_{lay}), as presented in Table 3. The back analysis process aims at determining the surface and layer elastic moduli as a function of the BBT deflection on top of each layer. The surface modulus is obtained by treating all layers as a single equivalent medium with composite stiffness and calculated using a homogenized semi-infinite elastic medium. The layers elastic moduli are obtained using LET considering each layer of the structure. For the BBT performed directly over the subgrade (Series A) specifically, the surface modulus is the same as the layer elastic modulus.

At each iteration, the modulus of the layer under analysis was adjusted until the deflection recorded in each BBT matched the target value. The sequence of the analysis proceeded from the lower to the upper layers: the moduli of the lower layers were obtained first for subsequent use in the moduli back analysis of the overlying layers. For example, the subgrade elastic modulus was first obtained using deflection results from Series A and then used to determine the CSS layer elastic modulus from Series B.

The thickness of each layer was predetermined based on the constructed experimental full-scale field tests and is summarized in Table 3. The applied load was consistent with that used for the BBT as detailed in Section 2.5. The Poisson's ratio of each layer was assumed based on values reported in the literature; they are dependent on the material characteristics presented in Table 3 [34–37]. For the geocell-reinforced layers, a Poisson's ratio of 0.25 was adopted as adopted by similar studies [11,38].

Surface elastic modulus (E_{suf})

Prediction of the surface elastic modulus (E_{suf}) is deemed relevant because it is related to the subgrade reaction modulus (K). Regardless of the number of layers, the surface elastic modulus, as does the subgrade reaction modulus, directly correlates the applied load on the surface to a deflection. The values of E_{suf} obtained from back analyses are shown in Table 3.

As shown in Table 3, the surface elastic moduli values, obtained during the construction of the layers, range from 23 to 76 MPa, with the lowest value associated with the subgrade. As comparatively stiffer layers were added during the construction process, the surface modulus is observed to increase. The back analyzed value of the subgrade surface modulus shown in Table 3 (23 MPa), is similar to values reported for materials characterized as silty clay [39,40].

The subsequent construction of the 250-mm CSS unreinforced layer resulted in a surface elastic modulus of 49 MPa, representing an

Table 2
BBT deflection results.

Series	Layer	Zone	Deflection Range (mm)	Average Deflection (mm)	COV (1)
A	Subgrade	1 to 4	1.15 to 6.29	3.05	36.3 %
B	CSS	1, 3 and 4	0.83 to 2.12	1.51	22.3 %
C	GBM	1 and 2	0.59 to 1.92	1.10	24.0 %
Bg	CSSg reinforced	2	1.31 to 1.78	1.51	10.3 %
Cg	GBMg reinforced	3 and 4	0.87 to 1.31	1.04	9.5 %

Table 3
Input parameters for each layer and moduli values back-analyzed from BBT average results.

Series	Layer	Zone	Thickness (mm)	Poisson's ratio (ν)	Surface moduli E_{suf} (MPa)	Layer elastic moduli E_{lay} (MPa)
A	Subgrade	1 to 4	∞	0.45	23	23
B	CSS	1, 3 and 4	250	0.35	49	283
C	GBM	1 and 2	150	0.35	67	215
Bg	CSSg reinforced	2	250	0.25	52	723
Cg	GBMg reinforced	3 and 4	150	0.25	76	656

improvement exceeding 100 %, as observed in results from using deflection data from the BBT test in Series B. This is because the CSS layer is more rigid than the subgrade. As the applied load is supported partially by this layer and partially by the subgrade, the deflection is reduced, resulting in a higher surface (equivalent) modulus. The same observation can be made for the BBT deflection of the 150-mm obtained from testing conducted on the unreinforced GBM layer (Series C), for which the surface modulus obtained was 67 MPa. This value is 190 % higher than the subgrade surface modulus and 36 % higher than the CSS surface modulus.

The reinforced zones, such as zone 2 to zone 4, demonstrated a similar pattern to control one (zone 1). However, a greater magnitude of the improvement could be observed. Use of geocells to reinforce the CSS layer (Test Series Bg) resulted in a surface elastic modulus of 52 MPa, which is 126 % higher than the subgrade surface modulus (Series A) and 6 % higher than the unreinforced CSS (Series B). The reinforced GBMg layer (Series Cg) yielded a surface elastic modulus of 76 MPa, which is 230 % higher than the subgrade surface modulus (Series A), 55 % higher than the CSS surface modulus (Series B) and 13 % higher than the unreinforced GBM surface modulus (Series C). It can therefore be concluded that the inclusion of a geocell reinforcement in a UGM layer can facilitate an increase in the surface modulus over the subgrade.

The E_{suf} result derives from field measurements of displacements in stages, meaning that the results are incremental. Consequently, direct quantitative comparison of the surface modulus of CSS and GBM is unrealistic due to the difference in each layer thickness and the fact that the GBM overlays the CSS. Only a qualitative comparison between surface modulus is appropriate, in addition to a comparison between the reinforced layer and its equivalent unreinforced one.

Layer elastic modulus (E_{lay})

The layer elastic moduli values obtained from back calculations are presented in Table 3. As the subgrade was considered a uniform elastic medium, Table 3 shows that from the BBT performed directly on the subgrade (Series A), the back analyzed modulus equaled 23 MPa – the same surface elastic modulus value obtained in the analyses presented in the previous section.

For the unreinforced CSS layer (Series B), Table 3 shows an elastic modulus of 283 MPa, obtained by considering an average of the deflections from zones 1, 3 and 4. Back calculation of the unreinforced CSS elastic modulus using only the individual BBT deflections for each zone resulted in 279, 308 and 263 MPa, respectively, for zones 1, 3 and 4, with a small dispersion among the results (COV less than 10 %). For the GBM unreinforced layer (Series C), the back analyzed elastic modulus obtained was 215 MPa considering the average BBT deflections from zones 1 and 2. Also in this case, the unreinforced GBM elastic modulus using only the individual BBT deflections was back-calculated, resulting in 206 and 223 MPa, respectively, with a small dispersion among the results (COV about 5 %).

The magnitudes of these back analyzed moduli are consistent with the ranges recommended by several studies and transportation agencies for typical CSS and GBM layers that classify as GP-GW by the USCS classification system [35,36,39,40]. Several MEPDM recommend an elastic modulus within a range of approximately 200 to 300 MPa for the aforementioned CSS and GBM, which is nearly identical to the range obtained in the experimental full-scale field test. The NCHRP 1-37A (2004) [32] recommends a range of 228 to 290 MPa (typical of 265 MPa) for these UGM. Saride et al. (2022) [15] reported an elastic modulus of 254 MPa for base layers based on long-term pavement performance. The Australian transportation guideline Austroads (2019) [33] suggests 250 MPa as a typical value for these materials, while the São Paulo City MEPDM manual IP-08 (2004) [30] indicates an approximate elastic modulus value of 250 MPa for CSS and GBM installed directly above the subgrade.

The results in Table 3 reveal that the use of a geocell reinforcement in the UGM significantly enhanced the layer elastic modulus. The back calculation for the reinforced layers (Series Bg and Cg) provided moduli of 723 and 656 MPa, respectively, for the CSSg and GBMg geocell-reinforced composite. For Series Cg (GBMg), the value of 656 MPa presented in Table 3 is the average of the back calculation of zones 3 and 4, the individual results for which were 593 and 719 MPa, respectively. The UGM elastic moduli in the geocell-reinforced zone showed significant improvement over the moduli obtained for the control zone, ranging from approximately 150 to 230 %, due to the confinement generated by the geocell reinforcement. Because the mechanical behavior of UGM is highly sensitive to its stress state, higher confinement led to higher strengths and stiffness, especially after larger compaction-induced stresses. A comparison of the moduli of unreinforced and reinforced layers are utilized to obtain the MIF and detailed in the next section.

Modulus improvement factor (MIF)

The MIF is a relevant parameter to quantify the improvement in a material from the inclusion of a geocell. Since it allows for direct consideration of the elastic modulus of a reinforced layer, using the MIF is probably the best approach to facilitate and to increase the inclusion of geocells as reinforcements in transportation infrastructure designs and works. In MEPDM analyses and evaluations, the reinforced modulus is obtained by multiplying the MIF by the unreinforced one (E_{ref} = MIF x E_{un}) so that only the improved elastic modulus and thickness are required as inputs for the reinforced layer.

Modulus improvement factor values were back calculated for the experimental full-scale test results for the CSS and GBM separately, and are presented in Table 4. Table 4 also shows information on the characteristics of the geocells used in the experiments: raw material, height, pocket size equivalent diameter, and wall stiffness (J). The MIF value for the CSS was calculated using the ratio between the reinforced elastic modulus from zone 2 and the average unreinforced elastic modulus from zones 1, 3 and 4. The MIF values for the GBM were calculated considering the reinforced moduli from zones 3 and 4 individually divided by the unreinforced elastic modulus average calculated from zones 1 and 2.

The results in Table 4 show an MIF ranging from 2.6 to 3.3 obtained for the three reinforced zones. The geocell-reinforced CSSg (Series Bg in zone 2) generated an MIF of 2.6, and the geocell-reinforced GBMg (Series Cg) generated MIFs of 2.8 and 3.3 for zones 3 and 4, respectively. Considering the previously discussed variation observed in the CSS unreinforced elastic modulus, with moduli equal to 279, 308 and 263 MPa for zones 1, 3 and 4, respectively, the geocell-reinforced MIF for this fill material was equal to 2.3, 2.6 and 2.7 for the same zones, respectively. These MIF values are very similar, particularly considering the inherent variability in an experimental full-scale field test conducted under less controlled conditions. The maximum absolute and relative differences were 0.4 and less than 10 %, respectively. In the case of GBM used as fill material, zones 1 and 2 produced unreinforced moduli respectively equal to 206 and 223 MPa, while an extreme range, between 2.7 and 3.5, was obtained for the geocell-reinforced MIF considering the smallest reinforced modulus with the highest unreinforced modulus and vice-versa. The calculated MIF results were within the range reported by several studies [11,15–18,25].

Comparatively higher MIF values were obtained for the geocell-reinforced mattress filled with GBM when compared to layers with CSS. This trend was expected since the MIF can be represented as a function of the soil-reinforcement relative stiffness index, S_i [13], defined as the ratio between the geocell wall stiffness (J) and the soil modulus number (k) in the hyperbolic constitutive soil model [42] multiplied by the atmosphere pressure (P_a) and the equivalent cell diameter (d_{eq}), as shown in Equation (2) below. The soil-reinforcement relative stiffness index is the most influential parameter for obtaining the MIF in direct proportionality. According to Garcia and Avesani Neto (2021) [13], a 10-fold increase in S_i can generate MIF increments greater

Table 4
MIF calculation from BBT test results reported by Zipoli and Avesani Neto (2022) [24] and predicted from Garcia and Avesani Neto (2021) [13] equation.

Study	Geocell			Infill material	MIF			
	Material	Height / equivalent diameter (mm)	J (kN/m)		Back analysis of experimental results			Analytical
					BBT[1]	PLT[1]	PLT[2]	Garcia and Avesani Neto (2021) [13]
This article	HDPE	150 / 192	1188	CSS	2.6	–	–	2.9
	HDPE	150 / 192	1188	GBM	2.8	–	–	3.2
	HDPE	150 / 192	1188	GBM	3.3	–	–	3.2
Zipoli and Avesani Neto (2022) [24]	NPA	120 / 178	1162	GBM	2.5	2.1	2.5	2.6

[1] Using ELLEA1 LET software.
[2] Using Avesani Neto's (2019) [12] two-layered elastic system solution.

than 60 %. As CSS is a more rigid material than GBM [36,39,41], the MIF for CSS is expected to be less than that for GBM.

$$S_i = \frac{2J}{kP_a d_{eq}} \quad (2)$$

Table 4 also presents MIF results reported by Zipoli and Avesani Neto (2022) [24] from a similar experimental full-scale field test performed on an airfield pavement structure to expand their comparison and analyses. The authors back calculated MIF from BBT and Plate Load Tests (PLT) using LET software and several two-layer elastic system solutions. The MIF reported in their study are comparable to those obtained herein, especially for the CSS as fill material [36,39,41]. The authors selected a different geocell for their field test, made of Novel Polymeric Alloy (NPA) and with distinct geometric characteristics, particularly height and thickness. A GBM with higher rigidity (greater soil modulus value) was also used to fill the cells.

The MIF value estimated using the analytical formulation proposed by Garcia and Avesani Neto (2021) [13] are also presented in Table 4. To calculate the MIF using this analytical method, CSS and GBM hyperbolic parameters were adopted based on in situ and laboratory tests and recommendations from the literature [42,43] as follows: $\gamma = 20$ kN/m^3, $c' = 0$, $\varphi' = 45°$, $R_f = 0.8$, $k = 900$ to CSS and 600 to GBM, $k_u/k = 1.2$ and $n = 0.4$. The geocell parameters and characteristics presented in Table 1 were adopted for the MIF analytical method. The stress generated by the compaction process was estimated using the methodology proposed by Ehrlich and Mitchell (1994) [37] considering procedures and equipment previously cited in Section 2.5.

As shown in Table 4, MIF values of 2.9 and 3.2 were obtained using the analytical method for geocell-reinforced CSS and GBM layers, respectively. These values are close to those obtained in the experimental full-scale field test. For the CSS, the absolute and relative differences between the MIF obtained from experiments and that calculated were 0.3 and 7 %, respectively. The absolute and relative differences between the MIF obtained from experiments and that calculated for the GBM were 0.1 to 0.4 and 3 to 13 %, respectively. Table 4 also shows the analytical MIF, calculated by Zipoli and Avesani Neto (2022) [24], as 2.6, which corresponds to their experimental field test. These results indicate a good prediction was provided by the analytical method.

Fig. 4 provides a comparison of the MIF values experimentally obtained with those analytically calculated for the experimental full-scale field test presented herein. The figure also shows the same comparison between experiments and calculated MIF results by other authors [13,25].

The results in Fig. 4 indicate a good agreement of the MIF values calculated using the analytical method with those obtained from

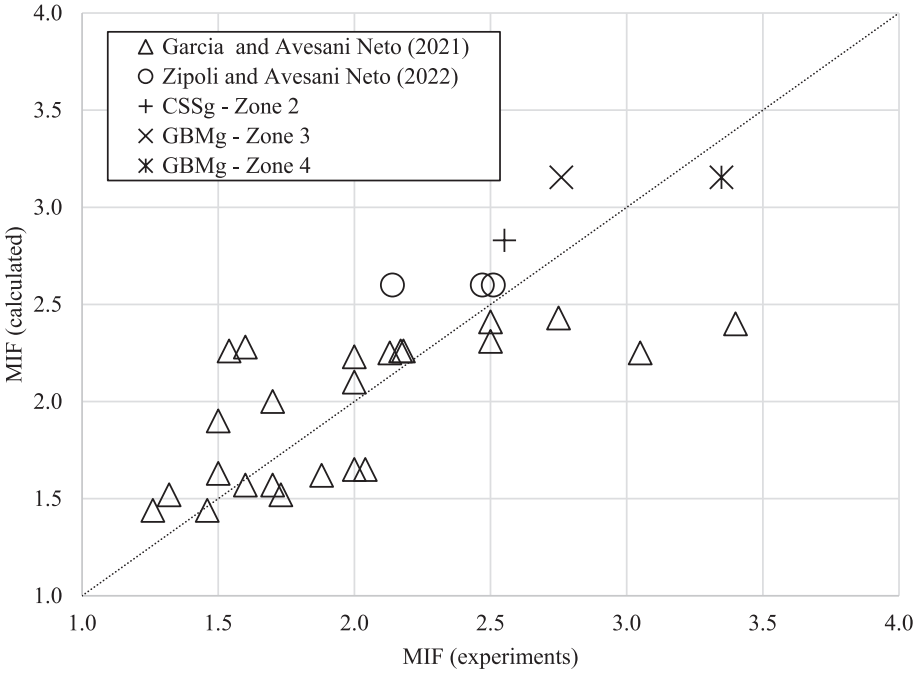

Fig. 4. Comparison of MIF obtained in experiments and calculated via analytical method by several authors.

experiments. Considering the significant variation in experimental conditions included in this plot, such as test type (laboratory, full-scale in the field and back analyzed works), applied load (static and cyclic PLT, BBT and FWD), geocell reinforcement characteristics (various raw materials, cell thickness, height and pocket size), fill soil (several types of sand, crushed rocks and coarse materials) and compaction conditions, it can be concluded that the analytical method satisfactorily estimated the MIF. The dashed reference line represents a perfect match between the experimental and calculated values (calculated MIF = experimental MIF). Most of the data from Garcia and Avesani Neto (2021) [13] (triangles) are distributed below the perfect match line, suggesting that the calculated MIF values are generally lower than the experimental ones. In contrast, the data from Zipoli and Avesani Neto (2022) [24] (circles) are closer to the equality line, indicating better agreement between the calculated and experimental MIFs. Regarding this study, the data from Zone 2 (CSSg) consistently shows calculated MIF values higher than the experimental ones. Meanwhile, in Zones 3 and 4 (GBMg), the experimental values exhibit variability, with one point near and other further from the perfect match line, reflecting a range of agreement between the calculated and experimental MIFs. Overall, the use of analytical formulations proves advantageous in determining the modulus of specific layers during rapid assessments or preliminary analyses in projects, especially for geocell reinforcement applications. Additionally, employing analytical solutions can facilitate obtaining the input parameters required for MEPDM software.

Conclusion

This article presented the back analyzed results from an experimental full-scale field test with unreinforced and geocell-reinforced layers subjected to in situ deflection experiments. The full-scale field test was performed on a highway test zone during construction. Two Unbound Granular Materials (UGM), a Crushed Stone Subbase (CSS) and Granular Base Material (GBM), of different thicknesses were utilized in the pavement structure layers. A geocell made with HDPE and measuring 150 mm in height was used as reinforcement for both fill materials. Four different 50-meter-long zones were constructed, one of which was unreinforced for control purposes and three of which were reinforced to evaluate the improvement from the geocell in the CSS and GBM layers. Deflection tests of all pavement structure layers were carried out using the Benkelman Beam Test (BBT). A total of 219 BBT were conducted across three different pavement structure layers/elevations, over the subgrade and the unreinforced and geocell-reinforced CSS and GBM layers. Based on the results from this investigation, the following conclusions can be made:

- Utilizing a geocell as pavement layers reinforcement led to a significant reduction in the deflection standard deviation. The deflection coefficient of variation was reduced to roughly 50 % in the UGM layers when the geocell was added, changing the layer classification from fair to very uniform.
- The use of a geocell reinforcement improved the surface elastic modulus of UGM layers over the subgrade. The surface modulus of the geocell-reinforced GBM was 230 % higher than the subgrade surface modulus and up to 13 % higher than the unreinforced GBM surface modulus.
- The UGM elastic moduli were significantly improved by the inclusion of the geocell reinforcement. The Modulus Improvement Factor (MIF) values were 2.6 for the CSS, and 2.8 and 3.3 for the GBM, all of which are in a range similar to that reported in the literature for comparable experiments.
- The theoretical MIF estimated using the analytical method showed good agreement with the results from the experimental full-scale field test, thus confirming the improved predictions of this approach.

The experimental test zone was incorporated into the highway pavement structure and has been monitored using Falling Weight Deflectometer (FWD) tests. In the future, back analyzed FWD results will be compared to the BBT results to evaluate the MIF and UGM performance over time.

CRediT authorship contribution statement

L.X. Feng: Writing – original draft, Software, Methodology, Investigation, Formal analysis, Data curation, Conceptualization. **J.O. Avesani Neto:** Writing – review & editing, Validation, Supervision, Project administration, Methodology, Formal analysis, Data curation, Conceptualization. **J.G. Zornberg:** Writing – review & editing.

Declaration of competing interest

The authors declare that they have no known competing financial interests or personal relationships that could have appeared to influence the work reported in this paper.

Acknowledgements

The authors would like to acknowledge that the original article was supported by the São Paulo Research Foundation (FAPESP - grant #2023/04447-1). The authors would also like to acknowledge the companies Geo Soluções, Strata India and Arteris Companies for performing the experimental full-scale field test.

Data availability

Data will be made available on request.

References

[1] Biswas S, Hussain M, Singh KL. Behavior of bamboo and jute geocell overlaying soft subgrade under repeated wheel loading. J Mater Civ Eng 2024;36. https://doi.org/10.1061/JMCEE7.MTENG-16528.
[2] Ghazvinian H, Karami H. Laboratory study of the effect of vegetation and gravel on runoff parameters under variable rainfall intensities. Water Sci Technol 2023;88:2424. https://doi.org/10.2166/wst.2023.352.
[3] Nurtjahjaningtyas I, Wicaksono LA, Shofi AMR. Modeling geocells as slope reinforcement using the limit equilibrium method. IOP Conf Ser Earth Environ Sci 2023;1249:012007. https://doi.org/10.1088/1755-1315/1249/1/012007.
[4] Krishnaraj P, Manju · G S, Gali ·, Latha M. Physical and Numerical Shaking Table Studies on Geocell-Reinforced Retaining Walls. International Journal of Geosynthetics and Ground Engineering 2023;9:62. DOI: 10.1007/s40891-023-00482-7.
[5] Sawada Y, Kitada M, Ling HI, Kawabata T. Lateral force–displacement relationships for shallowly buried pipe reinforced by geocells. Https://DoiOrg/101680/Jgein2200325 2023. DOI: 10.1680/JGEIN.22.00325.
[6] Amiri A, Moghaddas Tafreshi SN, Dawson AR. Vibration response of machine foundations protected by use of adjacent multi-layer geocells. Geotext Geomembr 2023;51:15–35. https://doi.org/10.1016/j.geotexmem.2023.03.001.
[7] Luo XW, Lu Z, Zhang JB, Yao HL. Study on performance of geocell-reinforced red clay subgrade. Https://DoiOrg/101680/Jgein2300068 2023:1–41. DOI: 10.1680/JGEIN.23.00068.
[8] Minchala D, Kuna KK, Gottumukkala BV, Pulikanti SP. Laboratory evaluation of marginal and industrial waste material in geocell-reinforced pavements under cyclic loading. J Test Eval 2024;52:20220627. https://doi.org/10.1520/JTE20220627.
[9] Khan A, Puppala AJ. Sustainable pavement with geocell reinforced Reclaimed-Asphalt-Pavement (RAP) base layer. J Clean Prod 2023;387:135802. https://doi.org/10.1016/j.jclepro.2022.135802.
[10] Punetha P, Nimbalkar S. Performance improvement of ballasted railway tracks using three-dimensional cellular geoinclusions. Geotext Geomembr 2022;50:1061–82. https://doi.org/10.1016/j.geotexmem.2022.06.007.
[11] Gottumukkala B, Mehar B, Minchala D, Pulikanti SP, Kuna KK. Laboratory and field evaluations of geocell reinforced bases for locally available material in the Himalayan Region. Int J Geosynth Ground Eng 2023;9. https://doi.org/10.1007/s40891-023-00497-0.
[12] Avesani Neto JO. Application of the two-layer system theory to calculate the settlements and vertical stress propagation in soil reinforcement with geocell. Geotext Geomembr 2019;47:32–41. https://doi.org/10.1016/j.geotexmem.2018.09.003.
[13] Garcia RS, Avesani Neto JO. Stress-dependent method for calculating the modulus improvement factor in geocell-reinforced soil layers. Geotext Geomembr 2021;49:146–58. https://doi.org/10.1016/j.geotexmem.2020.09.009.

[14] Zornberg JG. Functions and applications of geosynthetics in roadways. Transp Geotech Geoecol 2017;189:298–306. https://doi.org/10.1016/j.proeng.2017.05.048.
[15] Saride S, Asce M, Baadiga R, Asce SM, Balunaini U, Madhira MR. Modulus improvement factor-based design coefficients for geogrid- and geocell-reinforced bases. J Transp Eng, Part B: Pavements 2022;148. https://doi.org/10.1061/JPEODX.0000380.
[16] Mamatha KH, Dinesh SV, Dattatreya JK. Evaluation of flexural behaviour of geosynthetic-reinforced unbound granular material beams. Road Mater Pavement Des 2019;20:859–76. https://doi.org/10.1080/14680629.2017.1422790.
[17] Pokharel SK, Han J, Leshchinsky D, Parsons RL. Experimental evaluation of geocell-reinforced bases under repeated loading 2017. DOI: 10.1016/j.ijprt.2017.03.007.
[18] Ruge JC, Gonzalo Gomez J, Moreno CA. Analysis of the creep and the influence on the Modulus Improvement Factor (MIF) in polyolefin geocells using the stepped isothermal method. Geopolym Other Geosynth, IntechOpen 2020. https://doi.org/10.5772/intechopen.88518.
[19] Khan MA, Puppala AJ. Sustainable pavement with geocell reinforced reclaimed-asphalt-pavement (RAP) base layer. J Clean Prod 2023;387. https://doi.org/10.1016/j.jclepro.2022.135802.
[20] ASTM E2254-09. Standard Test Method for Storage Modulus Calibration of Dynamic Mechanical Analyzers. United States: 2018. DOI: 10.1520/E2254-09.
[21] ISO 6721-1. Plastics - Determination of Dynamic Mechanical Properties - Part 1: General Principles. Geneva, Switzerland: 2019.
[22] Strata Geosystems. Strata geocell - StrataWeb® HD - SW 330 to 712 - Data Sheet & Specifications 2020. https://www.strataglobal.com/wp-content/uploads/2021/08/StrataWeb-HD_SW-330-712_Datasheet.pdf (accessed December 11, 2023).
[23] Standards DNIT 141. Pavement - Granulometrically Stabilized Base - Service Specification. Brazil [in Portuguese]: 2010.
[24] ABNT NBR 11804. Materials for Granulometrically Stabilized Sub-base or Base for Pavements. Rio de Janeiro, Brazil [in Portuguese]: 1991.
[25] Zipoli LLR, Avesani Neto JO. Evaluation of back-calculated elastic moduli of unreinforced and geocell-reinforced unbound granular material from full-scale field tests. Geotext Geomembr 2022;50:910–21. https://doi.org/10.1016/j.geotexmem.2022.05.006.
[26] Giroud JP, Han J. Evaluation of the performance of unpaved roads incorporating geosynthetics - Planning. Geosynth Magaz 2016.
[27] AASHTO T 256-01. Standard Method of Test for Pavement Deflection Measurements. 2011.
[28] Lay MG. Planning and Pavements. Second. Gordon and Breach Publishers; 1990.
[29] Palmer LA, Barber ES. Soil Displacement Under a Circular Loaded Area. Highway Research Board Proceedings, vol. 20, Highway Research Board; 1940, p. 279–86.
[30] Odemark N. Investigations as to the elastic properties of solis and design of pavements according to the theory of elasticity. Statens Vaginst 1949;77.
[31] Levenberg E. ELLEA1: Isotropic Layered Elasticity in Excel: Pavement analysis tool for students and engineers - Excel spreadsheet. DTU Library 2016. https://orbit.dtu.dk/en/publications/ellea1-isotropic-layered-elasticity-in-excel-pavement-analysis-to (accessed December 3, 2023).
[32] Bahrani N, Levenberg E, Blanc J, Hornych P. General Rights Inverse Analysis of Pavement Layer Moduli Based on Data Collected by Buried Accelerometers and Geophones. Proceedings of 6th APT Conference, Springer; 2020, p. 592–601. DOI: 10.1007/978-3-030-55236-7_61.
[33] Avesani Neto JO, Rodrigues D. Instrumented load tests and layered elastic theory analysis of a large-scale EPS block embankment. Transp Geotech 2021;26. https://doi.org/10.1016/j.trgeo.2020.100442.
[34] Yoder EJ, Witczak MW. Principles of Pavement Design. London: Wiley; 1975. DOI: 10.1002/9780470172919.
[35] Wang Y, Leng Z, Wang G. Structural contribution of open-graded friction course mixes in mechanistic-empirical pavement design. Int J Pavement Eng 2014;15:731–41. https://doi.org/10.1080/10298436.2013.857776.
[36] Huang YH. Pavement Analysis and Design. Second. New Jersey: Pearson Education, Inc.; 2004.
[37] AASHTO. Mechanistic-Empirical Pavement Design Guide: A manual of practice. American Association of State Highway and Transportation Officials; 2008.
[38] Moghaddas Tafreshi SN, Shaghaghi T, Mehrjardi GT, Dawson AR, Ghadrdan M. A simplified method for predicting the settlement of circular footings on multi-layered geocell-reinforced non-cohesive soils. Geotext Geomembr 2015. https://doi.org/10.1016/j.geotexmem.2015.04.006.
[39] IP-08. Project Instruction IP-08: Mechanistic Analysis of Pavement Structure Fatigue. São Paulo, Brazil [in Portuguese]: 2004.
[40] U.S. Army Corps of Engineers. Design of Sheet Pile Cellular Structures Coffedams and Retaining Structures. Washington, D.C.: 1990.
[41] Austroads. Guide to Pavement Technology Part 2: Pavement Structural Design. Fourth. Sydney: Austroads LTD; 2019.
[42] Duncan JM, Byrne P, Wong KS, Mabry P. Strength, Stress-strain and Bulk Modulus Parameters for Finite Element Analyses of Stresses and Movements in Soil Masses. California: 1980.
[43] Ehrlich M, Mitchell JK. Working stress design method for reinforced soil walls. J Geotech Eng 1994;120.
[44] Baby LM, Avesani Neto JO. Evaluation of Geocell-Reinforced Railway Track Using FEM and FLM-Based Software: A Parametric Analysis. Int. J. of Geosynth. and Ground Eng. 2024;10:64. https://doi.org/10.1007/s40891-024-00564-0.